A unified intermediate and mechanism for soot combustion on potassium-supported oxides

Qian Li[1], Xiao Wang[1], Ying Xin[1], Zhaoliang Zhang[1], Yexin Zhang[2], Ce Hao[3], Ming Meng[4], Lirong Zheng[5] & Lei Zheng[5]

[1]School of Chemistry and Chemical Engineering, University of Jinan, Jinan 250022, China, [2]Ningbo Institute of Materials Technology & Engineering, Chinese Academy of Science, Ningbo 315201, China, [3]Faculty of Chemical, Environmental and Biological Science and Technology, Dalian University of Technology, Dalian 116024, China, [4]Tianjin Key Laboratory of Applied Catalysis Science & Engineering, School of Chemical Engineering & Technology, Tianjin University, Tianjin 300072, China, [5]Institute of High Energy Physics, Chinese Academy of Sciences, Beijing 100049, China.

The soot combustion mechanism over potassium-supported oxides (MgO, CeO_2 and ZrO_2) was studied to clarify the active sites and discover unified reaction intermediates in this typical gas-solid-solid catalytic reaction. The catalytically active sites were identified as free K^+ rather than K_2CO_3, which can activate gaseous oxygen. The active oxygen spills over to soot and forms a common intermediate, ketene, before it was further oxidized into the end product CO_2. The existence of ketene species was confirmed by density functional theory (DFT) calculations. The oxygen spillover mechanism is proposed, which is explained as an electron transfer from soot to gaseous oxygen through the active K^+ sites. The latter mechanism is confirmed for the first time since it was put forward in 1950, not only by ultraviolet photoelectron spectroscopy (UPS) results but also by semi-empirical theoretical calculations.

S oot (black carbon) from diesel engines has become a highly hazardous pollutant which can cause serious environmental and health problems[1]. Catalytic soot combustion is an efficient after-treatment for soot clean-up and also a relatively complex gas-solid-solid reaction, which has always been thought to operate by an oxygen-transfer mechanism. However, truly conclusive examples are rare. In 1950 the so-called electron-transfer mechanism was put forward, unfortunately no firm proof was available[2,3]. Although this was mentioned in a review paper in 2001[3], no further information is available. Therefore, it is important to clarify the two mechanisms and their relationship. In this context catalysts containing alkali metals and potassium (K) in particular were chosen due to their extremely high catalytic soot removal activity[4–7].

In most cases K is present to promote catalytic soot combustion and improve the contact of catalysts with soot and/or enhance the oxidation activity of the catalysts[8]. In addition K-compounds, for instance, K_2O, KOH and K_2CO_3, can serve as independent catalysts or active components of catalysts for soot combustion and have high activity[9]. It is well known that as opposed to precious metals and transition metals with variable valence states[10–15], K is present as K^+ in the catalyst, which cannot be reduced or oxidized during the redox reactions. How then can K-containing compounds catalyze an oxidation reaction like diesel soot combustion? Okubo *et al.* proposed carbonates on the surface of thermally treated K_2CO_3/Na-nepheline as the active species[16,17], possibly following the reaction of $K_2CO_3 + C + O_2 \rightarrow K_2O + 2CO_2$[18,19]. However, this is not a catalytic cycle[20]. The role of K was suggested to effectively participate in a redox cycle between K_xO_y and K_xO_{y+1}, though these K species did not correlate with activity[19,21–23]. Apart from the nature of the active sites, the reaction intermediates play an important role in the elucidation of the reaction mechanism. Ketene groups, a carbon–oxygen complex containing the structure of C=C=O, were first reported as intermediates for soot combustion on K/MgAlO catalysts in our previous work[24–26]. The question is whether ketene species are common reaction intermediates when K^+ is present?

In this work, we prepared different K-related species (K_2CO_3 and KO_x) on three typical oxides (MgO, CeO_2 and ZrO_2) by a single method using K_2CO_3 as the precursor. Not only the K^+ active sites but also a common intermediate were confirmed experimentally and theoretically. Thus an oxygen spillover mechanism including activation of gaseous oxygen, the formation and fate of ketene intermediates, and electron transfer processes was proposed.
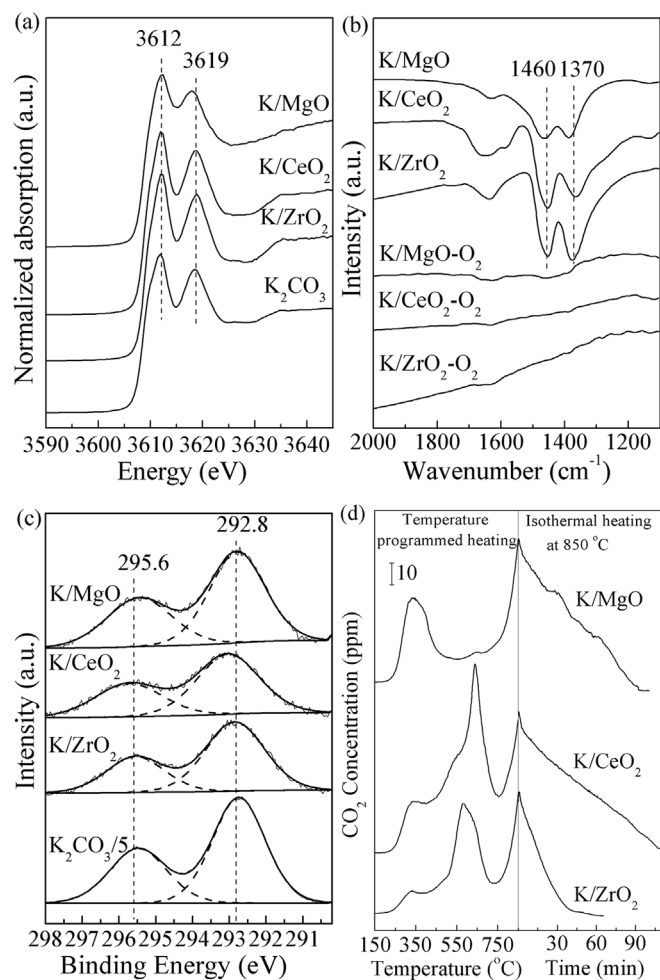
Figure 1 | (a) K K-edge normalized absorption, (b) IR spectra of fresh samples and the samples after O_2 treatment at 850°C for 2 h, (c) XPS spectra of K 2p for K/MgO, K/CeO$_2$, K/ZrO$_2$ and K$_2$CO$_3$, (d) CO$_2$–TPD patterns of K/MgO, K/CeO$_2$ and K/ZrO$_2$ heating from 150 to 850°C in He and holding at 850°C for 2 h.

Results

X-ray powder diffraction (XRD) patterns of K-supported oxides after calcination at 850°C for 2 h and exposure in air (K/MgO, K/CeO$_2$ and K/ZrO$_2$) show typical diffraction peaks of the corresponding single oxide, suggesting that the K species was present as a highly dispersed phase (Supplementary Figure S1, Supplementary Table S1 and S2). However, the normalized absorption spectra of K-edge of K in Figure 1a in K/MgO, K/CeO$_2$ and K/ZrO$_2$ are almost the same as that of K$_2$CO$_3$, showing two prominent peaks at 3612 and 3619 eV, similar to the results reported by Gomilšek et al.[27], which indicates that the K species was present as K$_2$CO$_3$. A small shift of the peak at 3619 eV for K/MgO may be associated with the formation of a small amount of K$_2$Mg(CO$_3$)$_2$·4H$_2$O, as observed for the same sample before calcinations (Supplementary Figure S2)[24]. No changes of oxides were observed after impregnation with K (Supplementary Figure S3). The presence of carbonate species can also be shown by IR spectra. As observed in Figure 1b, peaks at 1370 and 1460 cm^{-1} were observed, which are assigned to ν_1 and ν_4 of unidentate carbonate (–O–CO$_2$)[28]. Furthermore, X-ray photoelectron spectroscopy (XPS) spectra show two peaks at 295.6 and 292.8 eV, identical with that of K$_2$CO$_3$ (Figure 1c). It can be concluded that the K$_2$CO$_3$ phase on K/MgO, K/CeO$_2$ and K/ZrO$_2$ has been confirmed using the described preparation conditions.

Temperature-programmed desorption of CO$_2$ (CO$_2$–TPD) experiments (Figure 1d and Supplementary Figure S4) show that

the supported K$_2$CO$_3$ on MgO, CeO$_2$ and ZrO$_2$ has been completely decomposed after heat-treatment at 850°C for 2 h. As observed in Figure 1b, the IR peaks for the samples after O$_2$ treatment at 850°C for 2 h at 1370 and 1460 cm^{-1}, due to carbonates, disappeared. This would result in the formation of another K species, KO$_x$, following the decomposition of supported K$_2$CO$_3$. Combining the above results, two kinds of K species, K$_2$CO$_3$ and KO$_x$, have been successfully produced on the three typical oxides and these can be interconverted by desorption/adsorption of CO$_2$.

Discussion

Soot combustion in O$_2$ was carried out by temperature-programmed oxidation (TPO) reactions to evaluate catalytic activity, which was expressed in terms of T_m (Figure 2, Supplementary Figure S5 and Supplementary Table S1). It was observed that both the fresh samples and those after O$_2$ treatment exhibited almost the same T_m values. Furthermore, a weak CO$_2$ desorption (insets in Supplementary Figure S5) was observed at higher temperatures (> 700°C) for the fresh samples, which is attributed to the decomposition of K$_2$CO$_3$[24]. However, this is not the case for samples after O$_2$ treatment. This shows that in the TPO experiments over catalysts after O$_2$ treatment, the K-related phase is KO$_x$ rather than K$_2$CO$_3$. The TPO results confirmed that the KO$_x$ and K$_2$CO$_3$ species displayed almost the same catalytic activity. Specifically, in situ Laser Raman experiments (Supplementary Figure S6) also demonstrated that both K$_2$CO$_3$ and KO$_x$ can catalyze soot combustion reactions. In other words, no matter which K species is present, either K$_2$CO$_3$ or KO$_x$ in catalysts, the catalytically active sites are identified as K$^+$. This is highly important because K$_2$CO$_3$ was always thought to be responsible for soot combustion[16,17]. After water-washing, no catalytic activity is observable due to dissolution of the K$^+$ components (Supplementary Table S2)[24], confirming that free (isolated) K$^+$ is the active site. In order to exclude the effects of the support on soot combustion activity, SiO$_2$ as an inert substrate was chosen to demonstrate the role of K$^+$. It is showed that when K$_2$CO$_3$ was present (Supplementary Figure S7 and Figure S8), K/SiO$_2$ showed relatively high catalytic activity (Supplementary Figure S9), similar to that of K/MgO, K/CeO$_2$ and K/ZrO$_2$ (Figure 2). Thus, it can be confirmed that K$^+$ acts as an active site rather than a promoter.

Now, it is important to determine the origin of the active oxygen species in catalytic soot combustion when K$^+$ is present. For K-containing catalysts, the oxygen-transfer mechanism is the most important in which gaseous O$_2$ is activated by the alkali metal and then transferred to the carbon surface[24]. Both Janiak et al.[29] and Lamoen and Persson[30] proposed that K can enhance the affinity and dissociation of gaseous O$_2$, based on theoretical calculations. A similar view was presented by Jiménez et al. who found that the active oxygen on the catalyst for soot oxidation was increased by the presence of K$^+$[31]. However, the active oxygen species cannot be detected by temperature-programmed reduction (TPR) with H$_2$[24]. The existence of the active oxygen species needs to be confirmed by carefully designed experiments.

Soot–TPR results show that a certain amount of soot can be oxidized in the absence of O$_2$ (Figure 3a), suggesting the existence of active lattice oxygen in K/MgO, K/CeO$_2$ and K/ZrO$_2$. The activity of active lattice oxygen, as seen in Figure 3a inset, follows the order of K/ZrO$_2$>K/CeO$_2$>K/MgO, which is in the same order as the Sanderson electro-negativity of the corresponding supports (Supplementary Table S1). Because strong electro-negativity means strong electron attraction, strengthened chemical bonds of pure oxides with K$^+$ were formed, leading to weakening of the K–O bond in the catalysts. The Soot–TPR result is in good agreement with that of T_m from TPO (Supplementary Table S1, Figure 2 and Supplementary Figure S5). Additionally, it is noted that the strong CO$_2$ signal below 700°C and CO signal above 600°C for the bulk K$_2$CO$_3$ are ascribed to the
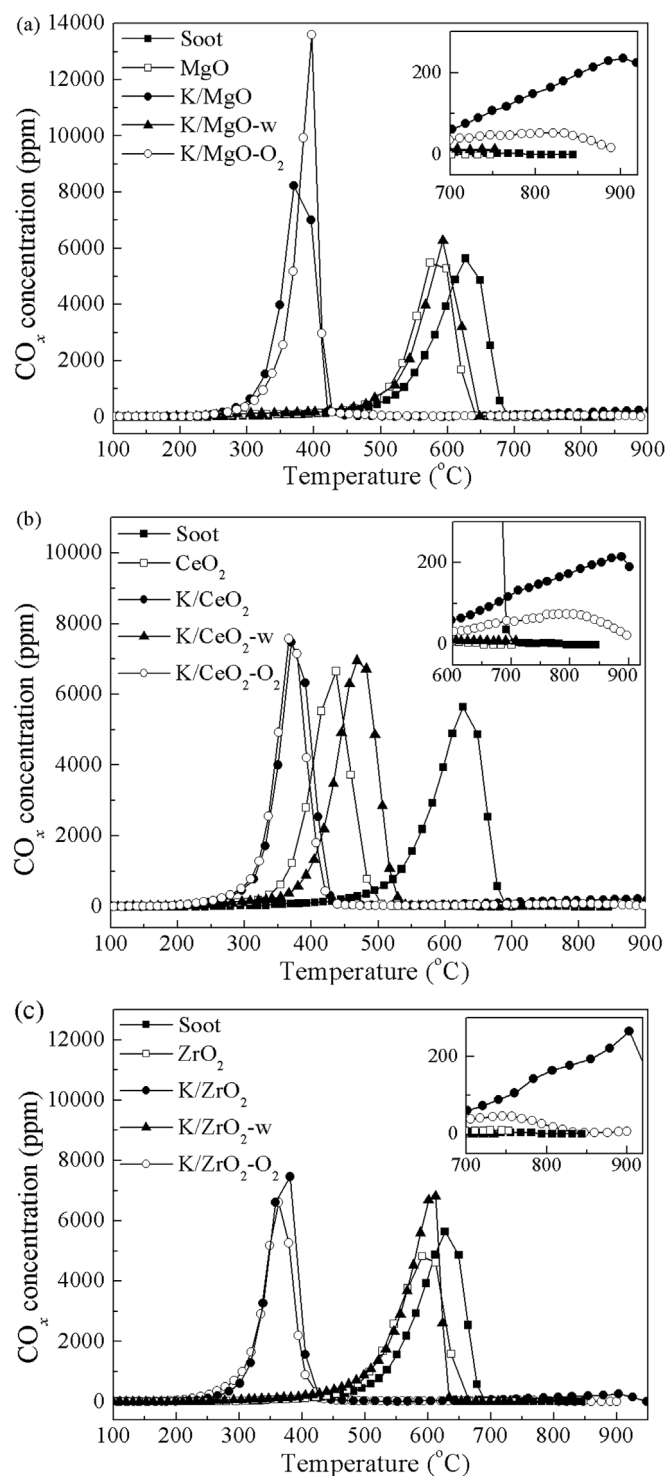
Figure 2 | TPO patterns of CO_x for soot combustion on pure oxides, K-supported oxides, K-supported samples after treatment in O_2 at 850°C for 2 h, and K-supported samples after water-washing treatment for 24 h: (a) MgO, (b) CeO_2 and (c) ZrO_2.

reactions of $K_2CO_3 + C \rightarrow K_2O + CO_2$ and $K_2CO_3 + 2C \rightarrow 2K + 3CO$ or $K_2O + C \rightarrow 2K + CO$, respectively[18,32].

In situ IR of NO adsorption was also performed, in which NO is used as a probing molecule, because NO can be efficiently stored on K^+ cation sites only after NO has been oxidized to NO_2[33,34]. First, the catalysts were pre-oxidized and then exposed to NO (Figure 3b and Supplementary Figure S10). A strong and stable peak at 1248 cm^{-1} is observed, which can be attributed to nitrite species derived from the
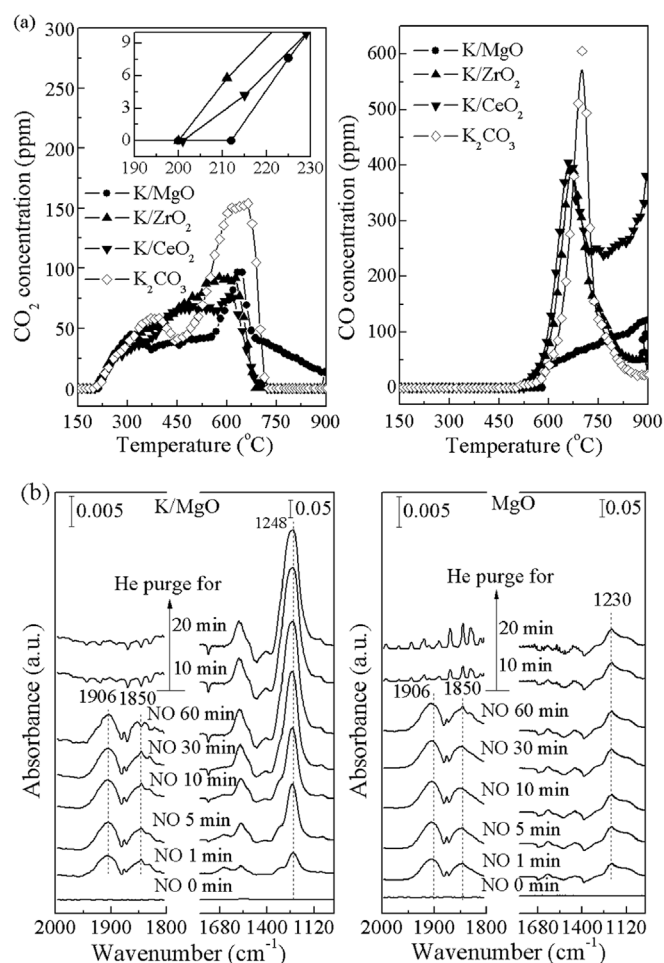

Figure 3 | (a) Soot–TPR for K/MgO, K/CeO_2, K/ZrO_2 and K_2CO_3 after O_2 treatment at 850°C for 2 h. The inset in (a) is the partially enlarged figure at low temperature range; (b) *In situ* IR spectra of NO adsorption (1000 ppm NO + He) on MgO and K/MgO at 100°C after O_2 treatment in 5 vol.% O_2 + He at 500°C for 30 min.

oxidation of NO by the active oxygen in the catalysts. However, over the corresponding potassium-free supports, only negligible peaks were present, possibly due to weak NO oxidation and adsorption. This is evidence of activation of gaseous O_2 on the active K^+ sites.

The role of activated O_2 was further confirmed by isothermal anaerobic titrations[35], in which the O_2 flow was turned on at first and then turned off during the catalytic soot combustion process (Supplementary Figure S11, Supplementary Table S1). The results showed that once the O_2 flow was stopped, the soot combustion activity gradually decreased, confirming the participation of active oxygen (O*) derived from gaseous O_2 in real reaction conditions (the O* amounts are listed in Table S1). Similar results have been demonstrated on Li-doped MgO, on which the $[Li^+O^-]$ active sites were formed from the interaction of Li^+ with molecular oxygen, which were responsible for the activity of methyl radical formation[36]. Moulijn and Kapteijn proposed that oxygen-containing reactant molecules were incorporated in or dissociated by a K-oxide cluster to produce an O* species with a relatively high reactivity for carbon and this oxygen species could be exchanged extremely quickly by gaseous oxygen-containing reactants, which is an example of oxygen spillover[37].

In situ IR experiments for soot combustion were carried out over K/MgO, K/CeO_2 and K/ZrO_2 (Figure 4a and Supplementary Figure S12). A characteristic IR band at 2162 cm^{-1} can be clearly observed, accompanied by the band at 2358 cm^{-1} and a series of bands in the
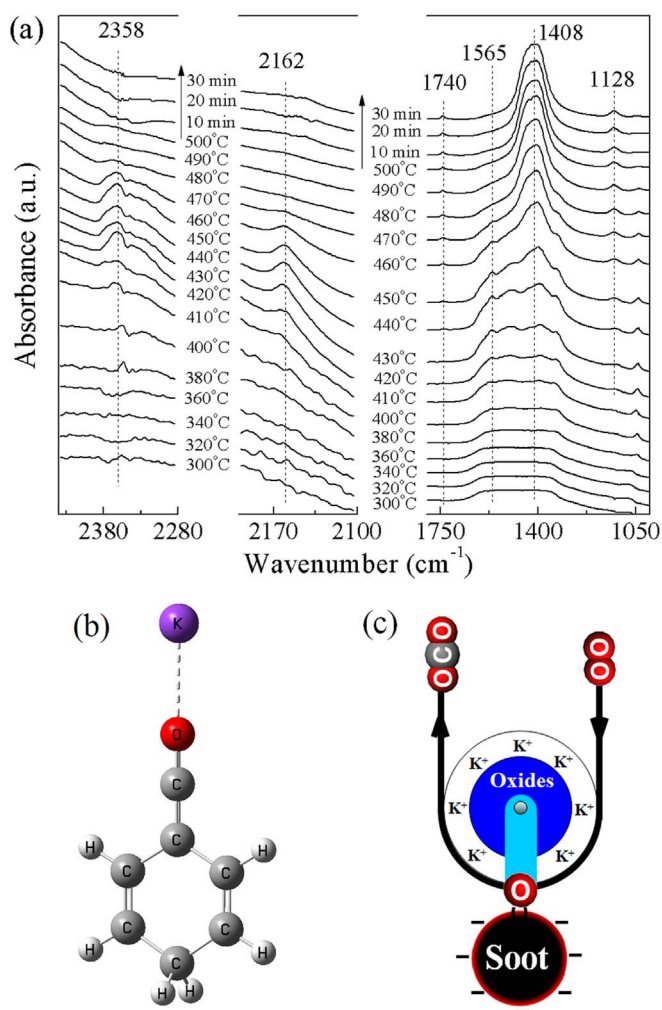
Figure 4 | (a) *In situ* IR spectra for soot combustion in a flow of 5 vol.% O_2 + He on K/MgO; (b) The optimized complex geometry of the quinonoid ketene molecule complex with K^+; (c) Illustration of the unified oxygen spillover and the common electron transfer process for soot combustion on potassium-supported oxides.

range of 1000–1800 cm^{-1}, which can be attributed to ketene species, physically adsorbed CO_2 and carbonate species, respectively. The assignment of ketene species can also be supported by density functional theory (DFT) calculations. Given that the true structure of the ketene intermediates is not known and the ketene group is formed from free carbon atoms of soot which possess structures similar to polycyclic aromatic hydrocarbons. The geometry of the quinonoid-ketene molecular complex with K^+ was optimized at the dispersion-corrected DFT level using the quantum program package Turbomole V6.4[38] and the IR vibration frequencies were thus calculated. The optimized structures are depicted in Figure 4b. The asymmetric stretch frequency of the ketene group for the complex quinonoid-ketene molecule has been calculated to be 2168 cm^{-1}, which is in good agreement with the experimental value, confirming the assignment of the peak at 2162 cm^{-1} to the ketene group is reasonable.

In view of the fact that the IR bands of the ketene group and CO_2-related species appeared simultaneously, the ketene species were deduced to be reaction intermediates during the soot combustion process. Further reaction of the ketene species was demonstrated by transient reactions and the corresponding *ex situ* IR, in which K/MgO was taken as the representative catalyst and the mixture of soot and K/MgO (1/9 weight ratio) was heated in O_2 to 350°C, then the O_2 flow was stopped (Supplementary Figure S13). In the 1st stage, soot

was oxidized to CO_x in O_2 while the temperature was increased to 350°C (a and b). In the 2nd stage the flow of O_2 was stopped at 350°C and the CO concentration sharply dropped to zero while the CO_2 concentration declined slowly, implying that some surface active oxygen on the catalyst transferred to the ketene group. As the evolution of CO_2 decreased to a negligible level, the ketene group disappeared, which can be shown from the vanishing of its characteristic peak at 2162 cm^{-1} in the inset in Figure S13 (c). These facts strongly support the transformation of the ketene species to CO_2 by active oxygen[24]. Since the appearance of the ketene species is independent of the catalyst support, it should be a unified reaction intermediate for K-supported catalysts. As shown (Figure 4c), the K^+ pulls O_2 from the gas phase and active oxygen species were obtained by the formation of KO_x ($[K^+O^-]$). The activated oxygen transfers to free carbon sites where the ketene intermediate is formed. This is further oxidized, by active oxygen, to form the end product CO_2. This is a typical oxygen spillover mechanism proposed by us[24] and others[39], in which the catalyst, as an oxygen carrier, can promote the transfer of oxygen from the gas phase to the carbon surface, by means of the formation of an intermediate compound.

Most importantly in this work, the electron-transfer mechanism was proved for the first time both by ultraviolet photoelectron spectroscopy (UPS) experiments and by theoretical calculations. The UPS spectra gave direct evidence of the changes in the electronic structures of soot due to the presence of the K^+ ions. As shown in Figure 5a, pure soot shows a broad UPS peak at approximately 9.0 eV, which is assigned to valence electrons of the p–σ bands on graphite soot[40,41]. This peak became weaker when soot was mixed with K/ZrO$_2$ (Figure 5a) or K/CeO$_2$ (Supplementary Figure S14a). However, the peak intensity of the mixtures of soot with supports (ZrO$_2$ or CeO$_2$) was nearly unchanged, indicating that the perturbations in the electronic properties of soot occur only in the presence of K^+ ions[42]. The absence of photoemission signals of soot for the mixtures of soot + K/MgO and soot + MgO is possibly due to the relatively low electrical conductivity properties of MgO (Supplementary Figure S14b). The perturbations in the electronic properties of soot mixed with K–supported samples can be illustrated by semi-empirical theoretical calculations. The contour plots of net charges for the soot model (graphene) and the mixtures of soot + catalyst are given in Figure 5b and c, respectively, which clearly describe the changes in the electronic structures due to the presence of K^+. The distribution of charges on pure soot is relatively homogeneous and the net charge is near to zero. When the K^+ ions are present, the net charge of the edge carbons is substantially changed. As shown in Figure 5c, the edge charges on soot become negative while the inner charges are mainly positive, regardless of the locations of the K^+ ions. This demonstrates an important role of the K^+ ions that attract the electrons from the inner carbon atoms to the edge carbon atoms and this is in agreement with the calculations of Yang *et al.*[43] The electron-rich carbon atoms favour donating electrons to the electrophilic species such as oxygen molecules to form active oxygen species such as O_2^- and O^-[44]. In other words, the K^+ ions facilitate the concentration of electrons on the soot surface with higher energy states, strengthening the driving force for efficient electron transfer from soot to O_2[45,46].

The electron transfer and the oxygen spillover mechanisms can be effectively integrated by the interaction of soot with the K^+ ions on K-supported catalysts[47]. On the one hand, the K^+ ions act on π electrons of soot and covalent K–C bonds may be present, leading to electron transfer from soot to the electronegative oxygen, thus decreasing the aromatic character of soot and activating gaseous oxygen[3,37]; On the other hand, the activated oxygen spills over from K^+ sites to soot and ketene species are formed, which weaken the neighbouring C–C bonds[3,37], and the product CO_x is evolved. The transfer of electrons from soot to K^+ was realized by way of oxygen species transferred from KO_x ($[K^+O^-]$) to soot.

4
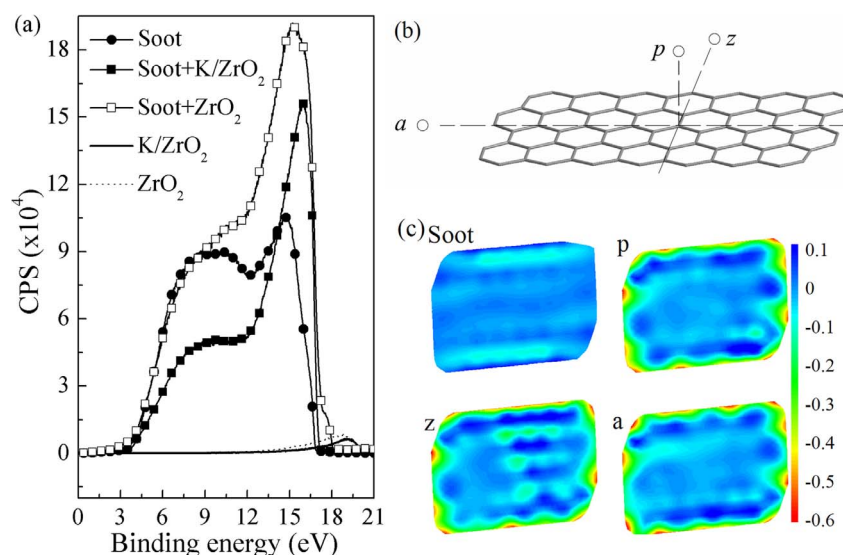
Figure 5 | (a) UP spectra of soot, K/ZrO_2 and soot + K/ZrO_2; (b) Graphene as the model structure of soot. Three locations of the K^+ ions near to the structures are labeled. Label p indicates the top location perpendicular to the plane of the soot model, while Labels z and a represent the locations on the same plane as the soot model, near to the zigzag edge and armchair edge of the soot, respectively; (c) Contour plots of net charges calculated by semi-empirical methods for soot and soot in the presence of the K^+ ion at the locations of p, z and a as referred to in (b).

In summary, for soot combustion on the K-supported catalysts, the following three conclusions have been made: (1) the catalytically active site has been identified as free K^+ rather than K_2CO_3; (2) the ketene intermediate has been found to be common to these processes; (3) the oxygen spillover mechanism has been interpreted as an intrinsic electron transfer process on an atomic scale through the active K^+ sites.

Methods

Catalyst preparation. The catalysts were prepared by impregnating single oxides (MgO, CeO_2 and ZrO_2) with the aqueous solution of K_2CO_3. Prior to the preparation, the oxides were heat-treated at 850°C for 2 h. Their suspensions in the aqueous solution of carbonate salt were evaporated while being stirred at 90°C until achieving a paste, which was then dried at 120°C overnight and calcined at 850°C for 2 h. In this way, the obtained catalysts with different support were designated as K/MgO, K/CeO_2 and K/ZrO_2. According to our previous work[24], the weight loading amount of K is determined as 8 wt.%. The as-prepared samples are also called as the fresh catalysts. Those after further O_2 treatment at 850°C for 2 h are denoted as $K/MgO–O_2$, $K/CeO_2–O_2$ and $K/ZrO_2–O_2$, respectively. While the samples after water-washing treatment were denoted as $K/MgO–w$, $K/CeO_2–w$ and $K/ZrO_2–w$, respectively, which were obtained by stirring the suspension of the fresh catalysts in the deionized water, then filtering, drying at 120°C overnight and calcinations at 850°C for 2 h.

Characterizations. Powder XRD patterns were recorded on a Rigaku D/max-rc diffractometer. Surface area and pore size distribution were determined by N_2 adsorption-desorption at 77 K with the BET method using a Micromeritics ASAP 2020 instrument after outgassing at 300°C for 5 h prior to analysis. XAFS measurements for the K K-edge were performed on the XAFS station of Beijing synchrotron radiation facility (BSRF, Beijing, China). K K-edge (3608 eV) data were collected at the 4B7A beam line of the Spectra in fluorescence mode with a Si (Li) detector. IR experiments were carried out using FT–IR spectrometer (Bruker Tensor 27) over 400–4000 cm^{-1} after 32 scans at a resolution of 4 cm^{-1}. The samples were diluted with KBr in the ratio of 1 : 100. XPS data were obtained on an AXIS–Ultra instrument from Kratos Analytical using monochromatic Al Kα radiation (225 W, 15 mA and 15 kV) and low-energy electron flooding for charge compensation. To compensate for surface charge effects, the binding energies were calibrated using the C 1s hydrocarbon peak at 284.80 eV. X–ray Fluorescence (XRF) experiments were performed on a ZSX Primus II instrument from Rigaku. Inductively Coupled Plasma-Atomic Emission Spectrometer (ICP-AES) experiments were carried out on the IRIS Intrepid IIXSP instrument from Thermo elemental. CO_2–TPD experiments were carried out in a fixed bed micro-reactor consisting of a quartz tube (6 mm i.d.). A 50 mg catalyst was pretreated in He (100 mL/min) at 850°C for 1 h and then cooled down to 250°C in He. When the temperature was stabilized at 250°C, 3976 ppm CO_2 in He (100 mL/min) was introduced. After saturation, the flow was switched to He (100 mL/min) to flush the sample to remove the weakly adsorbed species at 250°C and then cooled down to 150°C. Desorption was then conducted by heating the catalyst from 150 to 850°C at a ramp of 10°C/min in He (100 mL/min). At 850°C, the sample was isothermally heated until the completion of CO_2 desorption. The

desorbed CO_2 was detected by a quadruple mass spectrometer (MS, OminiStar 200, Balzers). The amount of CO_2 adsorbed at 250°C was calculated by the integration of the CO_2 desorption peaks. *In situ* Raman spectra were measured using a Raman spectroscope (HR800) with a CCD camera. The 632.8 nm line of a He–Ne laser was used to simulate the Raman spectra. The measurements were carried out with a microscope by using a ×50 objective lens (focus diameter larger than 1 micron) and the data were recorded in a backscattering geometry. Use of the cell allowed control of the sample temperature in static air at a heating rate of 5°C/min. UPS characterization was carried out using a HeI emission lamp (21.22 eV) as an excitation source and an analyzer resolution of 0.025 eV.

Activity tests. Temperature-programmed oxidation (TPO) reactions were conducted in the fixed bed micro-reactor. Printex–U from Degussa is used as the model soot. The soot was mixed with the catalyst in a weight ratio of 1 : 9 in an agate mortar for 30 min, which results in a tight contact between soot and catalyst. Isothermal reactions and isothermal anaerobic titrations were carried out to obtain the number of active redox sites (O* amount) and turnover frequency (TOF). Soot–TPR experiments were performed as the carbothermal reduction in the absence of gas phase oxygen in a fixed-bed flow reactor. The details for TPO experiments, isothermal reactions and isothermal anaerobic titrations, as well as Soot–TPR experiments are provided in supporting information.

In situ IR experiments. Soot combustion was further investigated using *in situ* IR spectroscopy. The IR spectra were recorded on the FT–IR spectrometer (Bruker Tensor 27) over 400–4000 cm^{-1} after 32 scans at a resolution of 4 cm^{-1}. Additionally, in order to confirm the existence of active oxygen species, *in situ* IR experiments for NO adsorption were performed. The experimental details are provided in supporting information.

DFT calculations and Semi-empirical quantum chemistry calculations. The geometry of the complex of quinonoid ketene molecular and K^+ was optimized at DFT levels using the well-known B3LYP hybrid exchange-correlation functional together with Ahlrichs split valence plus polarization (SVP) basis set for all atoms. A semi-empirical quantum chemistry program, MOPAC (Molecular Orbital Package) version 2012 was used to calculate the net charge of model soot based on NDDO (neglect of diatomic differential overlap) approximation. The program has been updated with a new and more accurate parameterization (PM7) for all the main group elements and transition metals. The details of calculation are provided in supporting information.

1. Gustafsson, Ö. M. *et al*. Brown clouds over South Asia: Biomass or fossil fuel combustion? *Science* **323**, 495–498 (2009).
2. Long, F. J. & Sykes, K. W. The catalysis of the oxidation of carbon. *J. Chim. Phys.* **47**, 361–378 (1950).
3. van Setten, B. A. A. L., Makkee, M. & Mou, J. A. Science and technology of catalytic diesel particulate filters, *Catal. Rev.* **43**, 489–564 (2001).
4. Jiménez, R., García, X., Cellie, C., Ruiz, P. & Gordon, A. L. Soot combustion with K/MgO as catalyst II. Effect of K-precursor. *Appl. Catal. A* **314**, 81–88 (2006).

5. Aneggi, E., de Leitenburg, C., Dolcetti, G. & Trovarelli, A. Diesel soot combustion activity of ceria promoted with alkali metals. *Catal. Today* **136**, 3–10 (2008).

6. Hleis, D., Labaki, M., Laversin, H., Courcot, D. & Aboukaïs, A. Comparison of alkali-promoted ZrO_2 catalysts towards carbon black oxidation. *Colloids and Surfaces A: Physicochem. Eng. Aspects* **330**, 193–200 (2008).

7. Zhang, Y. H., Zhang, Y. H., Xu, J. H., Jing, C. B. & Zhang, F. L. Studies of Al_2O_3–K catalysts prepared using various precursors for diesel soot elimination. *Thermochim. Acta* **468**, 15–20 (2008).

8. Sun, M. et al. The role of potassium in K/Co_3O_4 for soot combustion under loose contact. *Catal. Today* **175**, 100–105 (2011).

9. An, H. & Mcginn, P. J. Catalytic behavior of potassium containing compounds for diesel soot combustion. *Appl. Catal. B* **62**, 46–56 (2006).

10. Wu, X. D., Liu, S. & Weng, D. Effects of tungsten oxide on soot oxidation activity and sulfur poisoning resistance of Pt/Al_2O_3 catalyst. *Catal. Sci. Technol.* **1**, 644–651 (2011).

11. Wei, Y. C. et al. Highly active catalysts of gold nanoparticles supported on three-dimensionally ordered macroporous $LaFeO_3$ for soot oxidation. *Angew. Chem. Int. Ed.* **50**, 2326–2329 (2011).

12. López-Suárez, F. E. et al. Copper catalysts for soot oxidation: Alumina versus perovskite supports. *Environ. Sci. Technol.* **42**, 7670–7675 (2008).

13. Yu, Y. F., Meng, M. & Dai, F. F. The monolithic lawn-like CuO-based nanorods array used for diesel soot combustion under gravitational contact mode. *Nanoscale* **5**, 904–909 (2013).

14. Harrison, P. G. et al. Cobalt catalysts for the oxidation of diesel soot particulate. *Chem. Eng. J.* **95**, 47–55 (2003).

15. Guillén-Hurtado, N., García-García, A. & Bueno-López, A. Isotopic study of ceria-catalyzed soot oxidation in the presence of NO_x. *J. Catal.* **299**, 181–187 (2013).

16. Kimura, R., Elangovan, S. P., Ogura, M., Ushiyama, H. & Okubo, T. Alkali carbonate stabilized on aluminosilicate via solid ion exchange as a catalyst for diesel soot combustion. *J. Phys. Chem. C* **115**, 14892–14898 (2011).

17. Kimura, R., Wakabayashi, J., Elangovan, S. P., Ogura, M. & Okubo, T. Nepheline from K_2CO_3/nanosized sodalite as a prospective candidate for diesel soot combustion. *J. Am. Chem. Soc.* **130**, 12844–12845 (2008).

18. Matsukata, M., Fujikawa, T., Kikuchi, E. & Morita, Y. Interaction between potassium carbonate and carbon substrate at subgasification temperatures. Migration of potassium into the carbon matrix. *Energy Fuel* **2**, 750–756 (1988).

19. McKee, D. W. Chemistry and physics of carbon. *J. Chem. Phys.* **16**, 1–118 (1981).

20. Su, C. S. & McGinn, P. J. The effect of Ca^{2+} and Al^{3+} additions on the stability of potassium disilicate glass as a soot oxidation catalyst. *Appl. Catal. B* **138–139**, 70–78 (2013).

21. Gross, M. S., Ulla, M. A. & Querini, C. A. Catalytic oxidation of diesel soot: New characterization and kinetic evidence elated to the reaction mechanism on K/CeO_2 catalyst. *Appl. Catal. A* **360**, 81–88 (2009).

22. McKee, D. W. & Chatterji, D. The catalytic behavior of alkali metal carbonates and oxides in graphite oxidation reactions. *Carbon* **13**, 381–390 (1975).

23. Illán-Gómez, M. J., Linares-Solano, A., Radovic, L. R. & de Lecea, C. S. NO reduction by activated carbons. 2. Catalytic effect of potassium. *Energy Fuel* **9**, 97–103 (1995).

24. Zhang, Z. L., Zhang, Y. X., Wang, Z. P. & Gao, X. Y. Catalytic performance and mechanism of potassium-supported Mg–Al hydrotalcite mixed oxides for soot combustion with O_2. *J. Catal.* **271**, 12–21 (2010).

25. Zhang, Z. L. et al. Determination of intermediates and mechanism for soot combustion with NO_x/O_2 on potassium-supported Mg–Al hydrotalcite mixed oxides by in situ FTIR. *Environ. Sci. Technol.* **44**, 8254–8258 (2010).

26. Zhang, Y. X. et al. Determination of mechanism for soot oxidation with NO on potassium supported Mg–Al hydrotalcite mixed oxides. *Chem. Eng. Technol.* **34**, 1864–1868 (2011).

27. Gomilšek, J. P., Kodre, A., Arčon, I. & Nemanič, V. X-ray absorption in atomic potassium. *Nucl. Instr. and Meth. in Phys. Res. B* **266**, 677–680 (2008).

28. Thornton, E. W. & Harrison, P. G. Tin oxide surfaces Part 1.-Surface hydroxyl groups and the chemisorption of carbon dioxide and carbon monoxide on Tin (IV) oxide. *J. Chem. Soc., Faraday Trans.* **71**, 461–472 (1975).

29. Janiak, C., Hoffmann, R., Sjovall, P. & Kasemo, B. The potassium promoter function in the oxidation of graphite: an experimental and theoretical study. *Langmuir* **9**, 3427–3440 (1993).

30. Lamoen, D. & Persson, B. N. J. Adsorption of potassium and oxygen on graphite: A theoretical study. *J. Chem. Phys.* **108**, 3332–3341 (1998).

31. Jiménez, R., García, X., López, T. & Gordon, A. L. Catalytic combustion of soot. Effects of added alkali metals on CaO–MgO physical mixtures. *Fuel Process. Technol.* **89**, 1160–1168 (2008).

32. Moulijn, J. A., Cerfontain, M. B. & Kapteijn, F. Mechanism of the potassium catalysed gasification of carbon in CO_2*. *Fuel* **63**, 1043–1047 (1984).

33. Huang, Z. W. et al. A "smart" hollandite $deNO_x$ catalyst: Self-protection against alkali poisoning. *Angew. Chem. Int. Ed.* **52**, 660–664 (2013).

34. Wang, W. C. et al. Mixed-phase oxide catalyst based on Mn-mullite (Sm, Gd) Mn_2O_5 for NO oxidation in diesel exhaust. *Science* **337**, 832–835 (2012).

35. Zhang, Z. L., Han, D., Wei, S. J. & Zhang, Y. X. Determination of active site densities and mechanisms for soot combustion with O_2 on Fe-doped CeO_2 mixed oxides. *J. Catal.* **276**, 16–23 (2010).

36. Driscoll, D. J., Martir, W., Wang, J. X. & Lunsford, J. H. Formation of gas-phase methyl radicals over MgO. *J. Am. Chem. Soc.* **107**, 58–63 (1985).

37. Moulijn, J. A. & Kapteijn, F. K. Towards a unified theory of reactions of carbon with oxygen-containing molecules. *Carbon* **33**, 1155–1165 (1995).

38. Ahlrichs, R., Bär, M., Häser, M., Horn, H. & Kölmel, C. Electronic structure calculations on workstation computers: The program system turbomole. *Chem. Phys. Letters* **162**, 165–169 (1989).

39. Neumann, B., Kröger, C. & Fingas, E. Die wasserdampfzersetzung an Kohlenstoff mit aktivierenden zusätzen. *Z. Anorg. Chem.* **197**, 321–328 (1931).

40. Reinke, P., Garnier, M. G. & Oelhafen, P. J. In situ photoelectron spectroscopy analysis of tetrahedral amorphous carbon films. *Electron Spectrosc.* **136**, 239–245 (2004).

41. Colavita, P. E., Sun, B., Tse, K. & Hamers, R. J. Photochemical grafting of n-alkenes onto carbon surfaces: the role of photoelectron ejection. *J. Am. Chem. Soc.* **129**, 13554–13565 (2007).

42. Bruix, A. et al. A new type of strong metal–support interaction and the production of H_2 through the transformation of water on $Pt/CeO_2(111)$ and $Pt/CeO_x/TiO_2(110)$ catalysts. *J. Am. Chem. Soc.* **134**, 8968–8974 (2012).

43. Chen, S. G. & Yang, R. T. Unified mechanism of alkali and alkaline earth catalyzed gasification reactions of carbon by CO_2 and H_2O. *Energy Fuel* **11**, 421–427 (1997).

44. Wang, X., Zhang, Y. X., Li, Q., Wang, Z. P. & Zhang, Z. L. Identification of active oxygen species for soot combustion on $LaMnO_3$ perovskite. *Catal. Sci. Technol.* **2**, 1822–1824 (2012).

45. Matzner, S. & Boehm, H. P. Influence of nitrogen doping on the adsorption and reduction of nitric oxide by activated carbons. *Carbon* **36**, 1697–1709 (1998).

46. Wang, X. et al. Photocatalytic overall water splitting promoted by an α–β phase junction on Ga_2O_3. *Angew. Chem. Int. Ed.* **51**, 13089–13092 (2012).

47. Vayssilov, G. N. et al. J. Support nanostructure boosts oxygen transfer to catalytically active platinum nanoparticles. *Nat. Mater.* **10**, 310–315 (2011).

Acknowledgments

Author contributions

Q. L. designed and performed experiments. X. W. prepared the samples used in this work. Y. X. and Y. X. Z. helped synthesizing catalysts. Y. X. Z., L. R. Z. and L. Z. helped characterizing samples. Z. L. Z., C. H. and M. M. discussed the results. Q. L. and Z. L. Z. wrote the manuscript. Z. L. Z. supervised the project.

Additional information

Supplementary information accompanies this paper at http://www.nature.com/scientificreports

Competing financial interests: The authors declare no competing financial interests.

How to cite this article: Li, Q. et al. A unified intermediate and mechanism for soot combustion on potassium-supported oxides. *Sci. Rep.* **4**, 4725; DOI:10.1038/srep04725 (2014).